Lane change in flows through pillared microchannels

De, S.; van der Schaaf, J.; Deen, Niels G.; Kuipers, J. A.M.; Peters, E. A.J.F.; Padding, J. T.

DOI
10.1063/1.4995371

Publication date
2017

Document Version
Final published version

Published in
Physics of Fluids

Lane change in flows through pillared microchannels

Cite as: Phys. Fluids **29**, 113102 (2017); https://doi.org/10.1063/1.4995371
Submitted: 11 July 2017 . Accepted: 04 October 2017 . Published Online: 08 November 2017

S. De, J. van der Schaaf, N. G. Deen, J. A. M. Kuipers, E. A. J. F. Peters, and J. T. Padding

Lane change in flows through pillared microchannels

S. De,[1] J. van der Schaaf,[2] N. G. Deen,[3] J. A. M. Kuipers,[1]
E. A. J. F. Peters,[1] and J. T. Padding[4,a)]
[1]*Multiphase Reactors Group, Department of Chemical Engineering and Chemistry, Eindhoven University of Technology, Eindhoven, The Netherlands*
[2]*Chemical Reactor Engineering Group, Department of Chemical Engineering and Chemistry, Eindhoven University of Technology, Eindhoven, The Netherlands*
[3]*Multiphase and Reactive Flows Group, Department of Mechanical Engineering, Eindhoven University of Technology, Eindhoven, The Netherlands*
[4]*Process and Energy Department, Delft University of Technology, Delft, The Netherlands*

(Received 11 July 2017; accepted 4 October 2017; published online 8 November 2017)

It is known that viscoelastic fluids exhibit elastic instabilities in simple shear flow and flow with curved streamlines. During flow through a straight microchannel with pillars, we found strikingly strong hydrodynamic instabilities characterized by very large transversal excursions, even leading to a complete change in lanes, and the presence of fast and slow moving lanes. Particle image velocimetry measurements through a pillared microchannel provide experimental evidence of these instabilities at a very low Reynolds number (<0.01). The instability is characterized by a rapid increase in spatial and temporal fluctuations of velocity components and pressure at a critical Deborah number. We characterize under which conditions these strong instabilities arise. *Published by AIP Publishing.*
https://doi.org/10.1063/1.4995371

INTRODUCTION

Non-Newtonian fluids sometimes exhibit time dependent fluctuations in their flow fields that are reminiscent of turbulence, yet they occur under conditions where Newtonian fluids (with equivalent viscosity) display steady laminar flow.[1–7] The fluctuations occur when polymers, or other mesoscale objects present in viscoelastic fluids, are unable to respond sufficiently fast to changes in the fluid velocity field, leading to an elastic response. To quantify the flow conditions of viscoelastic fluids, two non-dimensional numbers play a significant role. First is the Reynolds number defined as $\mathrm{Re} = \frac{\rho U D}{\eta}$, where U is the average flow velocity, ρ is the fluid density, η is the zero shear viscosity, and D is a characteristic length scale. In microfluidic and porous media flows, the Reynolds number is usually very small. The other important dimensionless number is the Deborah number (De), which is the ratio of the (longest) relaxation time λ of the polymer and a characteristic time scale of the flow. This characteristic time scale is usually taken to be the time needed for the average flow to pass the characteristic length scale, so $De = \frac{\lambda U}{D}$. Elastic instabilities occur when the fluid is deformed so fast that spontaneous fluctuations in the velocity field keep growing instead of regressing back to zero. This is analogous, but not equal, to high velocity Newtonian flow around an object, where inertial instabilities appear beyond a critical Reynolds number.

A large amount of experimental and numerical work has been devoted to the study of elastic instabilities. Elastic instabilities have been observed by Poole *et al.*[1] and Arratia *et al.*[2] in cross-channel flow, by Pan *et al.*[3] in long straight microchannels with obstructions close to the inlet, and even in simple straight channels as reported by several researchers.[4–6] These observations have led to a number of numerical and theoretical works that try to reproduce or explain the instabilities. For example, Berti *et al.*[7] analyzed the Lyapunov exponent to characterize elastic instabilities, Morozov and Van Saarloos[8] performed a nonlinear stability analysis for planar Couette flow, and Pakdel and McKinley[9] developed a dimensionless criterion that characterizes the critical conditions for the onset of elastic instabilities in (two-dimensional) viscoelastic flows. The concept of elastic turbulence in relation with elastic instabilities for polymeric flow was really put forward in the seminal work of Groisman and Steinberg.[10,11] Burghelea *et al.*[12] showed that at low Reynolds numbers, the chaotic flow, caused by instabilities in viscoelastic flow through undulating channels, can be used for efficient mixing that is almost diffusion independent. Pakdel and McKinley[13] investigated viscoelastic lid driven cavity flow and reported conditions for flow instabilities. The onset of elastic instability in serpentine channels was studied numerically and experimentally by Zilz *et al.*[14] They showed that the streamline curvature is primarily responsible for three-dimensional elastic instabilities. McKinley *et al.*[15] experimentally observed viscoelastic flow instabilities in abrupt contractions, and attempts have been made to explain the observed nonlinear effects.[16,17] Elastic instabilities also lead to an enhanced pressure drop at high De numbers, as, for instance, reported for non-Newtonian fluids in contraction expansion flows.[18]

Although viscoelastic fluids in simple channel flows exhibit flow instabilities, the number of pore scale studies on viscoelastic flow through complex porous media is still limited. The onset of flow instability in a porous channel after a critical De number was studied for Boger fluids.[19,20] Recently

a)Author to whom correspondence should be addressed: J.T.Padding@tudelft.nl

Scholz *et al.*[21] reported enhanced dispersion of particles after a critical De number in a model porous medium using micro channels. The increase in apparent viscosity for viscoelastic fluids through a porous micro channel and the effect of elastic instability on residual oil recovery was studied.[22–25] They observed that velocity fluctuations at a high De number can instigate enhanced recovery. Very recently Machado *et al.*[26] studied viscoelastic flow through a microchannel and compared the experimental results with a pore network based model. Numerical simulations have been performed by several researchers for flow of non-Newtonian fluids through relatively simple and two-dimensional model porous media.[27–32] Mostly the simulations in complex geometries are limited to inelastic shear thinning fluids.[33,34] So a detailed understanding of the interaction between the fluid rheology and multiscale nature of the porous medium is still missing. The critical De number for the onset of such instabilities also varies significantly, which is complicated (or possibly caused) by the fact that there is no unique choice for the relevant length scale in the definition of the De number. Further, it is a matter of considerable debate, whether it is the extensional nature of the polymer or the (shear-induced) normal stress difference that is responsible for such instabilities in porous media. Our recent numerical work on viscoelastic flow through model porous medium shows that viscoelastic normal stress might play a very important role in instigating elastic instabilities.[35,36] Progress in microfluidic research enables us to study these intriguing flow features at length scales that are of significant importance in oil recovery, polymer processing, packed bed flows, blood flow though tissues, medicine, geology, and other applications.[37]

To obtain more insight into the rich and complex physics of viscoelastic fluid flow in porous media, in this paper, we will experimentally investigate the fascinating interplay of viscoelastic effects and pore structure in a pillared microchannel. Due to successive contraction and expansion caused by the pillars, the polymer molecules get elongated and relaxed repeatedly, leading to the buildup and release of elastic stresses. We observe that after a critical Deborah number (De), the flow becomes asymmetric, but the instabilities remain localized. At a higher De, the viscoelastic effects become so strong that the flow starts to *change from one pillar lane to another*. The extreme sideways motion is associated with large nonlinear, non-periodic instabilities. We also observe an increase in apparent viscosity along with the elastic turbulence that leads us to believe that these effects must be attributed to a significant extension of polymer chains. Newtonian solutions of equal (zero-shear) viscosity do not show such flow features. Our observations show that two different De numbers, one based on pillar diameter and another based on spacing between the pillars, are crucial to characterize the instability. Moreover, we try to explain how local spatial and temporal instabilities eventually lead to nonlocal instabilities with lane changes and elastic turbulence.

METHODOLOGY

Micro-PIV (particle image velocimetry) experiments are performed in long (6.6 cm) straight microchannels, with a width and height of 1 mm and 50 μm, respectively. The model porous medium is designed by placing an array of cylindrical pillars in a stretched hexagonal pattern from the beginning to the end of the channel as shown in Fig. 1. The channel and cylinders are etched in silicon. The distance along the flow direction (x) of the two successive pillars (X_P) and along the width (y) of the channel (Y_P) is shown in Table I for two different channels. The number of pillars along the x and y directions (n, m) is 1650 and 16, respectively, for channel 1 and 824 and 8 for channel 2. In this paper, we will mostly focus our results on experiments performed in channel 1 and use the other channel results for comparison. All pillars are modified with a hydrophilic coating and microchannels are fabricated using photolithography technique. A detailed description of the manufacturing of microchannel and properties is reported in the work of de Loos *et al.*[38,39]

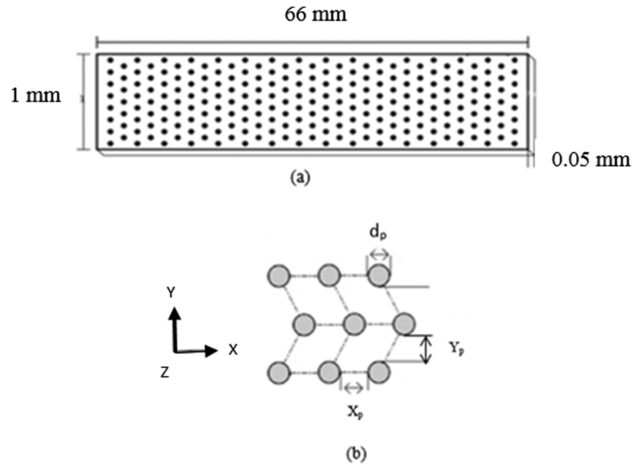

FIG. 1. Schematic drawing of the pillared microchannel. Flow is from left to right (x-direction). Planar walls are present at both sides in the width (y) and height (z) directions.

We investigated the flow of both a Newtonian fluid and a viscoelastic fluid through the pillared microchannel. A hydrolyzed polyacrylamide solution (HPAM, 20 MDa) is used as the viscoelastic fluid. The solution is prepared by adding 2000 ppm of HPAM 3630S and 0.5 wt.% salt (NaCl) in deionized water (brine) solution. The zero-shear viscosity (η_0) of the HPAM solution is 0.275 Pa s, as characterized by a standard strain controlled double gap rheometer (Anton Paar, MCR302) at room temperature (22 °C). The HPAM solution has a shear thinning rheology as shown in Fig. 2. At lower shear rates, a plateau region is observed (Newtonian like), followed by a shear thinning part. We have fitted the shear rheology data of the polymer with the Carreau-Yasuda model.[40] The Carreau-Yasuda model describes the Newtonian plateau and shear thinning behavior of HPAM

TABLE I. Dimensions of different micro channels used in this study.

Channel	Pillar diameter (μm) (D_P)	X-pitch (μm) (X_P)	Y-pitch (μm) (Y_P)
1	6	34	28.6
2	12	68	57.2

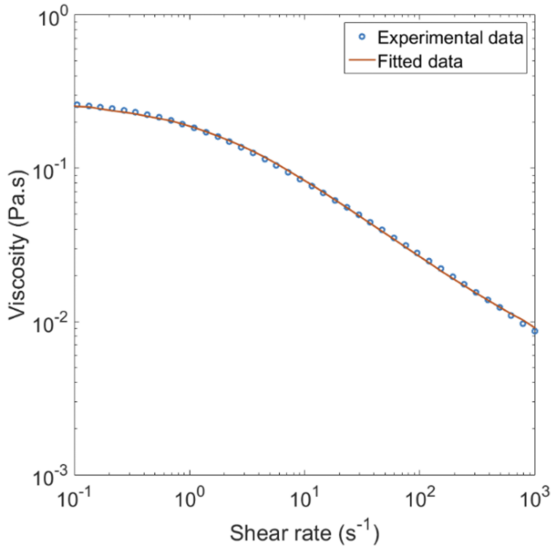

FIG. 2. Shear rheology data of HPAM.

accurately,

$$\eta\left(\dot{\gamma}\right) - \eta_\infty = (\eta_0 - \eta_\infty)\left[1 + \left(\lambda\,\dot{\gamma}\right)^a\right]^{\frac{(n-1)}{a}}, \qquad (1)$$

where λ represents the relaxation time, η_∞ is the infinite shear viscosity, n is the power law index, and a is a parameter describing the range of the transition from the Newtonian plateau to the power law region.

The parameters obtained from the fit are $a = 0.88 \pm 0.06$, $n = 0.497 \pm 0.006$, and $\lambda = 1.00 \pm 0.05$ s. The low value of n (relative to $n = 1$ for a Newtonian fluid) shows the highly shear thinning nature of this polymer solution.

The rheological characterization of similar HPAM solution has been done in detail in the recent work of Howe *et al.*[23] For all our experiments, we have kept the Reynolds number $\mathrm{Re} = \frac{\rho U D_P}{\eta}$ less than 0.01 (even when η is taken to be η_∞, the water viscosity), so any inertial effects can be neglected. Here D_P is the pillar diameter. We will introduce two different De numbers based on two relevant length scales. The De number with regard to the pillar diameter as the characteristic length is defined as $De_P = \frac{\lambda U}{D_P}$, and the De number with respect to the pillar-to-pillar distance (X-pitch) is defined as $De_L = \frac{\lambda U}{X_P}$. Both De numbers are relevant because the polymers experience curved and contraction-expansion flow when passing each single pillar, which has a large influence on the polymer conformation if De_p is sufficiently large, while the polymers have time to relax their conformations during their flow in between the pillars if De_L is sufficiently low.

In our microchannel experiments, we investigate different De numbers by slowly changing the flow rate of the injected HPAM solution using a KR Analytical syringe pump. This pump can provide a very low steady flow rate, so the Reynolds number is kept low. A Sensor Technics micro pressure sensor (Puchheim, Germany) is connected to the channel so the pressure drop over the channel can be measured. The range is 0-2 bars, with a temporal resolution of 1 ms. At low flow rates, it is possible to reach a steady pressure. At higher flow rates, the pressure signal has much more fluctuations. When this happens, we wait until the statistical characteristics of the pressure fluctuations become constant (i.e., when a statistical steady state is achieved) before performing other measurements. A statistical steady state is defined when the statistical characteristics (a windowed average and standard deviation) of the fluctuations become constant.

The pillared microchannel is placed on a Zeiss Axio Observer D1, which is an inverted microscope. To visualize the flow, the fluid is seeded with 1 μm fluorescent tracer particles (Nile red, Molecular probes, Invitrogen, density: 1055 kg/m^3, excitation range 535–575 nm, 0.02 wt.%). In our experiments, tracer particle concentration of 0.02 wt.% was found to be optimum as larger particle concentrations lead to agglomeration issues. Images are captured using a Redlake Motion Pro X-4 camera mounted on the top of the microscope. The experimental setup is similar to the setup described in the work of Sousa *et al.*[41] The depth of the field of the microscope was calculated to be 10% of the height of the microchannel. We visualize the path lines in a focal plane in the central plane between the top and bottom walls to decrease any effect of out of plane velocity gradients, laterally in a square section (around 66% of the channel width) close to the middle section along the channel, to decrease any effects of the side walls and inlet and outlet. Bright field images are captured at a frame rate of 30 fps, which is much faster than the time scale of the fluid flow. However, for higher flow rates at De > 1, a higher frame rate of 60 fps is used. We use a high intensity directed light source to excite the tracer particles. A green filter (500–600 nm) is used to filter any other light except the light from the particles.

Images from the camera were processed using Davis (version 8.2.0) and Matlab software (version R2015a) packages. Vector plots were created from the image sets using PIV time series sum of correlation, after subtracting the average to remove any stagnant particles from the image. A mask was created from a picture of the channel using visible light. This mask was then applied to the image sets, and velocity vectors were calculated. We have performed a series of experiments to verify the reproducibility of the experimental data points.

RESULTS

Figures 3(a) and 3(b) show the time averaged and spatial averaged standard deviation of velocity along the flow direction (x) for different Deborah numbers, expressed in terms of De_L. The first standard deviation characterizes spatial fluctuations of velocities, while the second one characterizes the temporal fluctuations. For each time frame, we first determine a time-dependent spatial standard deviation $\sigma_v(t) = \sqrt{\overline{v^2(t)} - \overline{v(t)}^2}$ characterizing the spatial variation of velocities (the overbar signifies spatial averaging). Then we perform a temporal averaging $\langle\sigma_v(t)\rangle$ of the obtained standard deviations for each De number (angular brackets signify temporal averaging). Note that the velocity field is *always* spatially inhomogeneous, even for a Newtonian fluid. However, for a Newtonian fluid in the creeping limit, the spatially dependent velocity field scales linearly with the overall (average) flow velocity. Therefore, to highlight non-Newtonian features, we divide the measured standard deviation by the average flow velocity.

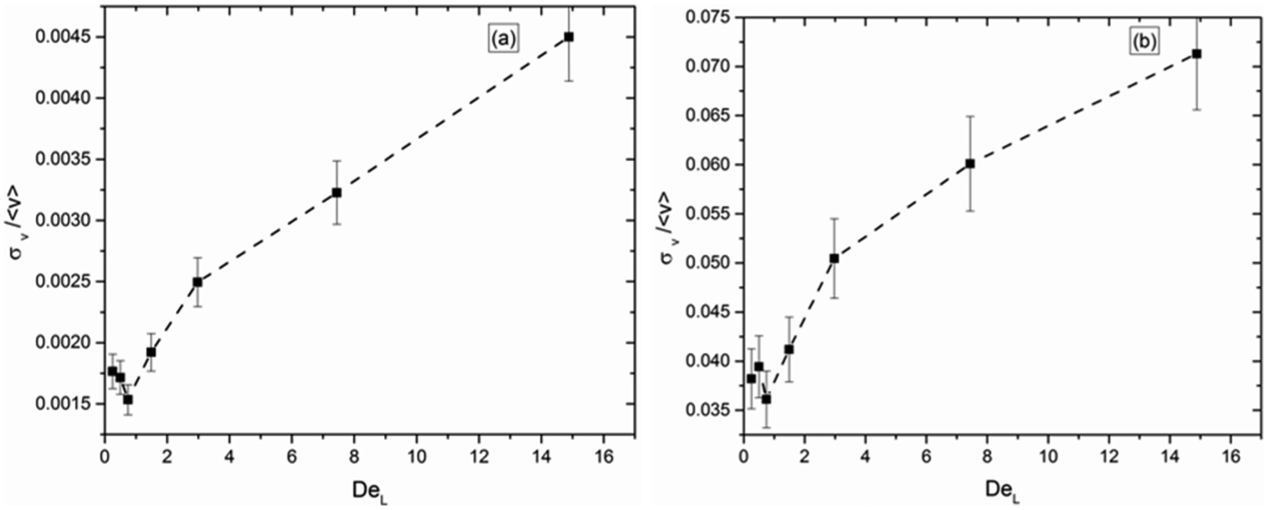

FIG. 3. (a) Time-averaged spatial standard deviation of the velocity normalized by the average flow velocity vs. Deborah number De_L; (b) spatially averaged temporal standard deviation of the velocity normalized by the average flow velocity vs. Deborah number De_L.

In the second case, for each point in the flow domain, we first determine a spatially dependent standard deviation $\sigma_v(x,y) = \sqrt{\langle v^2(x,y)\rangle - \langle v(x,y)\rangle^2}$ characterizing the temporal fluctuations of velocities at that location. Then we perform a spatial averaging $\overline{\sigma_v(x,y)}$ of the obtained standard deviations for each De number. We divide this standard deviation also by the average flow velocity.

Figure 3(a) shows that the time-averaged spatial velocity standard deviation normalized by the average flow velocity is constant (within error bars) up to $De_L = 1.5$. This indicates the amount of "base" fluctuations that are present in the system for (near-)Newtonian flows, as detected at the level of the interrogation areas used in our PIV method. However, for $De_L = 3.0$ and higher, we find that the fluctuations grow faster than would be expected for a Newtonian fluid. Figure 3(b) shows that the spatially averaged temporal velocity standard deviation normalized by the average flow velocity similarly changes from constant to growing at a similar De number.

The above observations show that the velocity fluctuations in the pillared microchannel are both temporal and spatial in nature and that they change in character at a critical (pitch-based) De_L number between 1.5 and 3. This is also clearly observed in time sequences of our μ-PIV images, where the onset of a flow asymmetry is clearly visible as the flow lines start to deviate from a regular laminar profile beyond $De_L = 1.5$. After $De_L = 1.5$, we observe strong flow asymmetries, ultimately accompanied with crossover of flow into neighboring channels (explained later).

Note that no such instabilities occur in Newtonian fluids for both channels at comparable flow rates; the normalized velocity fluctuations remain at a constant low level, independent of flow rate.

Next we investigate the evolution of the standard deviation of streamwise velocity components, as a function of the position along the channel length. To this end, we divide the whole flow domain under consideration into 100 consecutive areas and determine the time-averaged spatial velocity fluctuations for each area. Normalizing for each flow rate by the time averaged standard deviations at the entrance of the observation region, we can assess whether the velocity fluctuations remain constant or increase as the fluid flows through the channel.

Figure 4 gives a measure about the typical number of pillars (along the x-direction), around which the flow undergoes a continuous contraction–expansion, to develop such instabilities after the critical De number is reached. The long time averaged pressure profiles obtained in our experiments also supports these velocity fluctuation observations.

The power spectrum profiles corresponding to the streamwise and lateral velocity fluctuations are shown in Fig. 5. We observe that both power spectra are relatively flat at lower

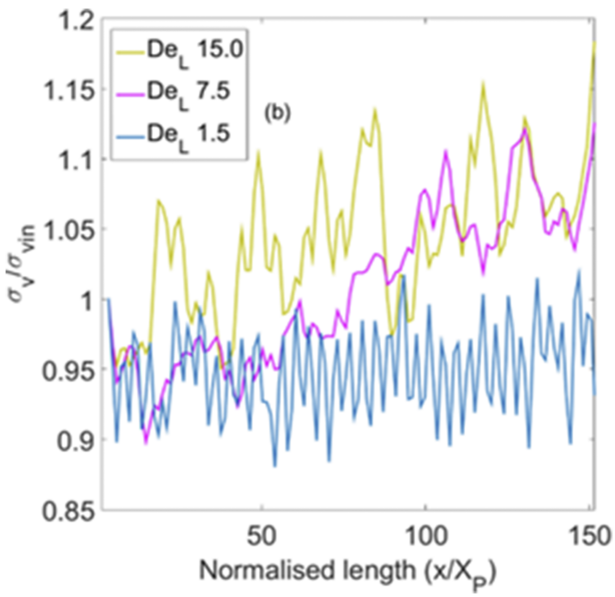

FIG. 4. Streamwise standard deviation of the velocity, normalized by standard deviation at the entrance of the observation region ($x = 0$) as a function of position (normalized by the x-pitch) along the channel length. Different colors correspond to different Deborah numbers (De_L).

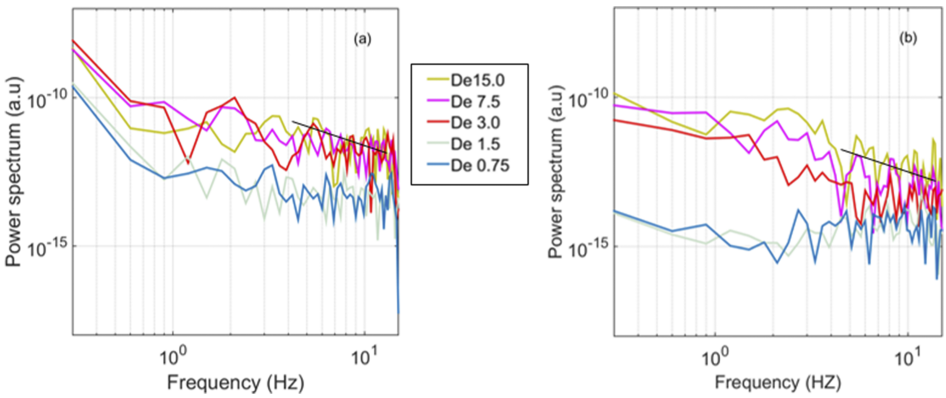

FIG. 5. (a) Power spectrum of streamwise velocity fluctuations. (b) Power spectrum of lateral velocity fluctuations.

De numbers (Newtonian regime) but shift up after a certain critical De number. This shift is most clearly visible for the lateral velocity fluctuations at low frequencies. Although the data are too noisy to make definitive measurements of power law exponents, we find that the spectra at higher De numbers are consistent with power law behavior for high frequencies with an exponent of around −3, in agreement with observations in the recent literature.[3,42] This power law dependence in such a broad range of spatial and temporal frequencies means that the fluid motion is excited at different spatial and temporal scales. A high power indicates the presence of strong low frequency fluctuations. Interestingly, the exponent is much larger than the Kolmogorov exponent of −5/3, found for velocity spectra of high Re inertial turbulence. This means that the nature of the fluctuation is essentially different.

We note that the apparent increase in power occurring at the lowest frequency is probably erroneous. This lowest frequency equals 1/T, where T is the total measurement time of the experiment. Since the sine wave corresponding to that frequency is only sampled once, the accuracy of the Fourier transform at this lowest frequency is very poor. Neglecting this first point, in Figs. 5(a) and 5(b), we observe a flat spectrum over almost the entire frequency range for low De numbers.

Experiments have also been performed in micro channels with a larger X-pitch (68 μm), which thus have larger porosity compared with the previous channel of 34 μm. We again observe a non-monotonous response of the velocity fluctuations to flow velocity; however, now the response is shifted to larger flow velocities. Figure 6 shows that if we represent the time averaged velocity fluctuations (total standard deviation normalized by the average flow velocity) versus the De number with respect to the pitch, De_L, then the onset of instability occurs at the approximately same critical De_L between 1.5 and 3.0. This is related to the fact that the pillar to pitch ratio is kept constant in both the microchannels (Table I).

In both micro channels, we find that below the critical Deborah number between 1.5 and 3.0, the fluid flow is still relatively stable, in the sense that the flow is keeping to its own lane through the pillar geometry. Figure 7 shows time-averaged velocity fields (averaged over 100 successive images) for De numbers below and above this critical number. Figure 7(a) shows that the time averaged velocity vectors for De_L 0.5 are nearly uniform. Figure 7(b) shows a non-uniform flow field from lane to lane at De_L 2.0. The appearance of a slow and fast co-moving flow field is clearly observed in Fig. 7(c) (De_L 3.0). At De_L around 10 [Fig. 7(d)], two phenomena are observed. Along with the slow and fast moving lanes, a sideways crossover of flow from one to another channel occurs. These crossover flows are transient and appear (and disappear) in a non-periodic way at apparently random locations. The fact that one of these transversal flows is visible even in the time averaged velocity fields [boxed in Fig. 7(d)] shows that these fluctuations can have a very low frequency of appearance and disappearance. The reader is referred to the videos in the supplementary material for an impression (note that because of the imaging system, the flow appears to move from right to left in the videos). Recently, Scholz *et al.*[21] and Machado *et al.*[26] reported asymmetric streamlines at high viscoelasticity in the flow through microchannels that have a different flow configuration. However, in our case, the instability arises at a much lower De number, with very strong lateral migration and spatio-temporal fluctuations not reported earlier.

These interesting observations can be explained as caused by elastic instabilities, if we take into account both the time

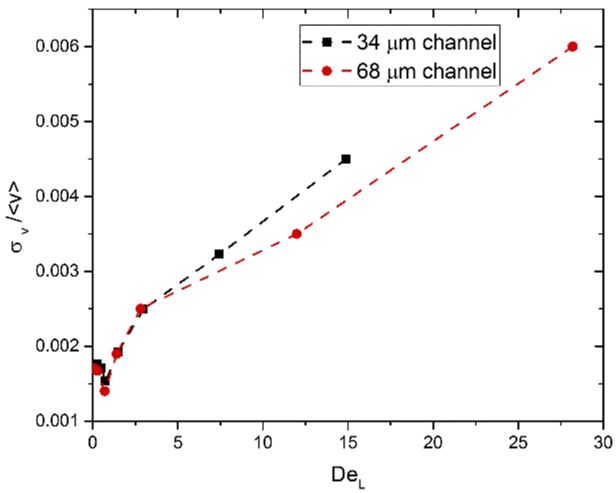

FIG. 6. Time averaged velocity fluctuations vs. Deborah number De_L total fluctuating magnitude normalized by the average flow velocity for 34 and 68 μm channel.

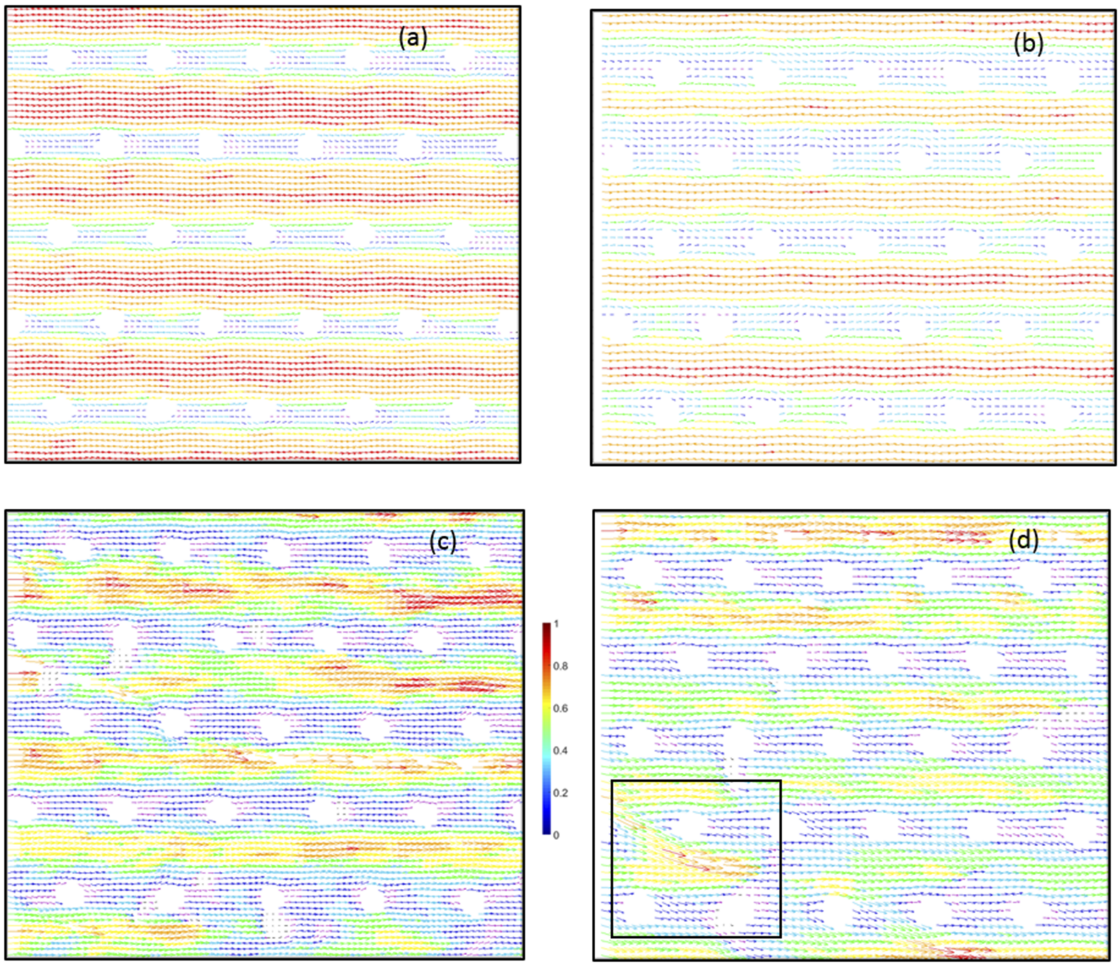

FIG. 7. Time averaged velocity profiles (normalized) at (a) De_L 0.5, (b) De_L 2.0, (c) De_L 3.0, and (d) De_L 10.0 (arrows show the flow direction in the domain, blue to red code shows the lowest to highest normalized velocity magnitude). Average is over 100 successive images.

scales of flow across a single cylinder (De_P) and across the pitch (De_L). According to Table I, channel 1 has the highest confinement. At lower flow rates (<0.2 μl/min), the polymer intrinsic relaxation time is less than both these flow time scales. Hence the polymers can easily relax while flowing between two successive pillars. At a critical flow rate of 0.2 μl/min, the De_P becomes of the order of 10, but De_L is still less than 2. Thus, the polymers cannot fully relax while crossing the pillars, but nevertheless they can relax between two consecutive pillars. The local viscoelastic stresses that develop near the pillars may cause short lived instabilities, causing flow asymmetry. However, when the flow rate is more than 0.9 μl/min, both De_P and De_L become larger than 2.5. In that case, the viscoelastic stresses become long lived and nonlinear (both spatially and temporally), and elastic turbulence sets in. This stress imbalance creates a certain flow resistance in the flow paths, forcing the polymers to change to a less resistance (sideways) path. Unlike Kawale *et al.*,[43] we observe a very strong lateral migration with spatio-temporal fluctuations as discussed in the earlier section, with the simultaneous presence of fast and slow moving lanes.

As mentioned, the observed sideway crossover is non-periodic in nature and occurs far away from the walls. Also, the elastic instability is accompanied by an increase in apparent relative viscosity, defined as the ratio of the pressure drop and flow rate for the viscoelastic fluid compared with that ratio for a Newtonian fluid of the same zero shear viscosity. Although from bulk rheology measurement we confirmed that our fluid is shear thinning at all measurable rates, we see an increase in apparent viscosity in both the channels when the Deborah number is around 10, as shown in Fig. 8. A plateau of apparent relative viscosity is expected at a low De number. The plateau and the onset of instability at a critical De between 1.5 and 3.0 is not captured by the pressure drop measurements as they occur at relatively lower flow rates and is in the lower limits of the pressure sensors to measure accurately. However, at around De 10, when strong elastic instability associated with a change in flow lanes sets in, the apparent viscosity starts to increase. Due to the stronger confinement effects, we observe that the rate of shear thinning of the polymer is faster in the 34 μm channel compared with the 68 μm channel.

In our pillared microchannel, the polymer undergoes continuous contraction and expansion. At higher viscoelasticity, the polymer does not get sufficient time to relax. So the viscoelastic stresses build up. These normal stresses and especially the 1st normal stress difference (N_1) might play

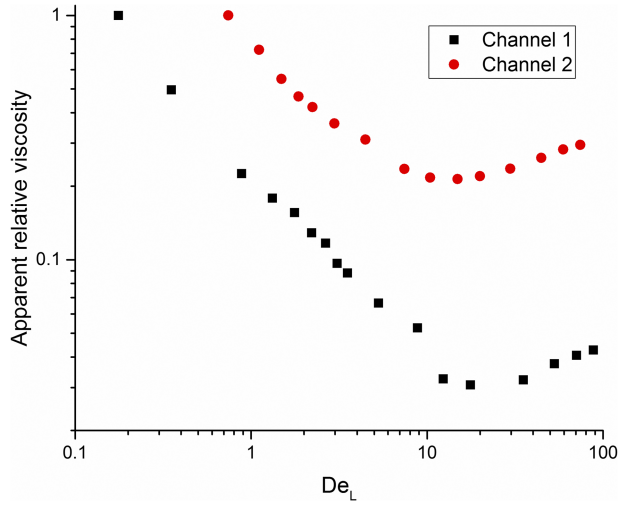

FIG. 8. Plot of normalized pressure drop across the pillared channel as a function of a De_L number for 34 μm and 68 μm channel.

a very important role in driving the strong spatio-temporal fluctuations, leading to elastic instabilities.[35,44]

CONCLUSION AND OUTLOOK

In summary, this experimental work shows evidence that placement of pillars in a straight microfluidic channel, even at relatively high porosity, has a strong effect on the development of elastic instabilities. We observe very interesting flow structures with increased viscoelasticity having both temporal and spatial fluctuations, with strong crossflow motion and the presence of fast and slow co-moving lanes. Such strong crossflow motion can be used to enhance mixing, which without the pillars is very cumbersome for such generally highly viscous fluids. Other snakelike microchannels have also been used to enhance mixing, but these channels have a higher surface to volume ratio, leading to an even higher pressure drop. We also showed that two different De numbers, one based on pillar diameter and another based on pitch, are required to characterize the flow instability. However, the De number based on the pitch overall seems to be the best to indicate large scale instabilities. A detailed flow analysis shows that these instabilities are significantly different from instabilities observed in simple shear flow, which appear at relatively larger De numbers[3] compared with our findings. This work provides an outlook to study flow and mixing through complex, random, and real porous media.

SUPPLEMENTARY MATERIAL

See supplementary material for videos of viscoelastic flow through a micropillared channel at De_L 0.25, 7.5, and 15, respectively. Note that because of the imaging system, the flow in these videos is from right to left.

ACKNOWLEDGMENTS

This work is part of the Industrial Partnership Programme (IPP) "Computational sciences for energy research" of the Foundation for Fundamental Research on Matter (FOM), which is part of the Netherlands Organisation for Scientific Research (NWO). This research programme is co-financed by Shell Global Solutions International B.V. We would also like to thank Paul Van Bussel for his contribution to the work.

[1] R. J. Poole, M. A. Alves, and P. J. Oliveira, "Purely elastic flow asymmetries," Phys. Rev. Lett. **99**, 164503 (2007).
[2] P. E. Arratia, C. C. Thomas, J. Diorio, and J. P. Gollub, "Elastic instabilities of polymer solutions in cross-channel flow," Phys. Rev. Lett. **96**, 144502 (2006).
[3] L. Pan, A. Morozov, C. Wagner, and P. E. Arratia, "Nonlinear elastic instability in channel flows at low Reynolds numbers," Phys. Rev. Lett. **110**, 174502 (2013).
[4] H. Bodiguel, J. Beaumont, A. Machado, L. Martinie, H. Kellay, and A. Colin, "Flow enhancement due to elastic turbulence in channel flows of shear thinning fluids," Phys. Rev. Lett. **114**, 028302 (2015).
[5] J. Tai, C. P. Lim, and Y. C. Lam, "Visualization of polymer relaxation in viscoelastic turbulent micro-channel flow," Sci. Rep. **5**, 16633 (2015).
[6] D. Bonn, F. Ingremeau, Y. Amarouchene, and H. Kellay, "Large velocity fluctuations in small-Reynolds-number pipe flow of polymer solutions," Phys. Rev. E **84**(R), 045301 (2011).
[7] S. Berti, A. Bistagnino, G. Boffetta, A. Celani, and S. Musacchio, "Two-dimensional elastic turbulence," Phys. Rev. E **77**(R), 055306 (2008).
[8] A. N. Morozov and W. Van Saarloos, "Subcritical finite-amplitude solutions for plane Couette flow of viscoelastic fluids," Phys. Rev. Lett. **95**, 024501 (2005).
[9] P. Pakdel and G. McKinley, "Elastic instability and curved streamlines," Phys. Rev. Lett. **77**, 2459 (1996).
[10] A. Groisman and V. Steinberg, "Elastic turbulence in a polymer solution flow," Nature **405**, 53 (2000).
[11] A. Groisman and V. Steinberg, "Elastic turbulence in curvilinear flows of polymer solutions," New J. Phys. **6**, 29 (2004).
[12] T. Burghelea, E. Segre, I. Bar-Joseph, A. Groisman, and V. Steinberg, "Chaotic flow and efficient mixing in a microchannel with a polymer solution," Phys. Rev. E **69**, 066305 (2004).
[13] P. Pakdel and G. H. McKinley, "Cavity flows of elastic liquids: Purely elastic instabilities," Phys. Fluids **10**, 1058 (1998).
[14] J. Zilz, R. J. Poole, M. A. Alves, D. Bartolo, B. Levache, and A. Lindner, "Geometric scaling of a purely elastic flow instability in serpentine channels," J. Fluid Mech. **712**, 203 (2012).
[15] G. H. McKinley, W. P. Raiford, R. A. Brown, and R. C. Armstrong, "Nonlinear dynamics of viscoelastic flow in axisymmetric abrupt contractions," J. Fluid Mech. **223**, 411 (1991).
[16] R. G. Larson, "Instabilities in viscoelastic flows," Rheol. Acta **31**, 213 (1992).
[17] E. S. Shaqfeh, "Purely elastic instabilities in viscometric flows," Annu. Rev. Fluid Mech. **28**, 129 (1996).
[18] J. P. Rothstein and G. H. McKinley, "The axisymmetric contraction-expansion: The role of extensional rheology on vortex growth dynamics and the enhanced pressure drop," J. Non-Newtonian Fluid Mech. **98**(1), 33 (2001).
[19] B. Khomami and L. D. Moreno, "Stability of viscoelastic flow around periodic arrays of cylinders," Rheol. Acta **36**, 367 (1997).
[20] D. F. James, R. Yip, and I. G. Currie, "Slow flow of Boger fluids through model fibrous porous media," J. Rheol. **56**, 1249 (2012).
[21] C. Scholz, F. Wirner, J. R. Gomez-Solano, and C. Bechinger, "Enhanced dispersion by elastic turbulence in porous media," Europhys. Lett. **107**, 54003 (2014).
[22] A. M. Howe, A. Clarke, and D. Giernalczyk, "Flow of concentrated viscoelastic polymer solutions in porous media: Effect of MW and concentration on elastic turbulence onset in various geometries," Soft Matter **11**, 6419 (2015).
[23] A. Clarke, A. M. Howe, J. Mitchell, J. Staniland, L. Hawkes, and K. Leeper, "Mechanism of anomalously increased oil displacement with aqueous viscoelastic polymer solutions," Soft Matter **11**, 3536 (2015).
[24] M. A. Nilsson, R. Kulkarni, L. Gerberich, R. Hammond, R. Singh, E. Baumhoff, and J. P. Rothstein, "Effect of fluid rheology on enhanced oil recovery in a microfluidic sandstone device," J. Non-Newtonian Fluid Mech. **202**, 112 (2013).
[25] J. Mitchell, K. Lyons, A. M. Howe, and A. Clarke, "Viscoelastic polymer flows and elastic turbulence in three-dimensional porous structures," Soft Matter **12**, 460 (2016).

[26]A. Machado, H. Bodiguel, J. Beaumont, G. Clisson, and A. Colin, "Extra dissipation and flow uniformization due to elastic instabilities of shear-thinning polymer solutions in model porous media," Biomicrofluidics **10**, 043507 (2016).
[27]T. Sochi, "Pore-scale modeling of viscoelastic flow in porous media using a Bautista-Manero fluid," Int. J. Heat Fluid Flow **30**, 1202 (2009).
[28]A. W. Liu, D. E. Bornside, R. C. Armstrong, and R. A. Brown, "Viscoelastic flow of polymer solutions around a periodic, linear array of cylinders: Comparisons of predictions for microstructure and flow fields," J. Non-Newtonian Fluid Mech. **77**, 153 (1998).
[29]D. Richter, G. Iaccarino, and E. S. G. Shaqfeh, "Simulations of three-dimensional viscoelastic flows past a circular cylinder at moderate Reynolds numbers," J. Fluid Mech. **651**, 415 (2010).
[30]K. K. Talwar and B. Khomami, "Flow of viscoelastic fluids past periodic square arrays of cylinders: Inertial and shear thinning viscosity and elasticity effects," J. Non-Newtonian Fluid Mech. **57**, 177 (1995).
[31]R. J. Marshall and A. B. Metzner, "Flow of viscoelastic fluids through porous media," Ind. Eng. Chem. Fundam. **6**, 393 (1967).
[32]S. De, S. Das, J. A. M. Kuipers, E. A. J. F. Peters, and J. T. Padding, "A coupled finite volume immersed boundary method for simulating 3D viscoelastic flows in complex geometries," J. Non-Newtonian Fluid Mech. **232**, 67 (2016).
[33]J. P. Singh, S. Padhy, E. S. G. Shaqfeh, and D. L. Koch, "Flow of power-law fluids in fixed beds of cylinders or spheres," J. Fluid Mech. **713**, 491 (2012).
[34]S. Shahsavari and G. H. McKinley, "Mobility and pore-scale fluid dynamics of rate-dependent yield-stress fluids flowing through fibrous porous media," J. Non-Newtonian Fluid Mech. **235**, 76 (2016).
[35]S. De, J. A. M. Kuipers, E. A. J. F. Peters, and J. T. Padding, "Viscoelastic flow simulations in model porous media," Phys. Rev. Fluids **2**, 53303 (2017).
[36]S. De, J. A. M. Kuipers, E. A. J. F. Peters, and J. T. Padding, "Viscoelastic flow simulations in random porous media," J. Non-Newtonian Fluid Mech. **248**, 50 (2017).
[37]F. A. L. Dullien, *Porous Media-Fluid Transport and Pore Structure* (Academic, New York, 1979).
[38]S. R. A. de Loos, "Smart micro reactors: Carbon nano fibers and pillars in micro channels reactor design, synthesis and mass transfer," Ph.D. thesis, TU Eindhoven, 2012.
[39]S. R. A. de Loos, J. van der Schaaf, R. M. Tiggelaar, T. A. Nijhuis, M. H. J. M. De Croon, and J. C. Schouten, "Gas-liquid dynamics at low Reynolds numbers in pillared rectangular micro channels," Microfluid. Nanofluid. **9**, 131 (2010).
[40]R. B. Bird, R. C. Armstrong, and O. Hassager, *Dynamics of Polymeric Liquids*, Volume 1: Fluid Mechanics, 2nd ed. (Wiley, 1987).
[41]P. C. Sousa, F. T. Pinho, M. S. N. Oliveira, and M. A. Alves, "Efficient microfluidic rectifiers for viscoelastic fluid flow," J. Non-Newtonian Fluid Mech. **165**, 652 (2010).
[42]M. Grilli, A. V. Quesada, and M. Ellero, "Transition to turbulence and mixing in a viscoelastic fluid flowing inside a channel with a periodic array of cylindrical obstacles," Phys. Rev. Lett. **110**, 174501 (2013).
[43]D. Kawale, E. Marques, P. L. J. Zitha, M. T. Kreutzer, W. R. Rossen, and P. E. Boukany, "Elastic instabilities during the flow of hydrolyzed polyacrylamide solution in porous media: Effect of pore-shape and salt," Soft Matter **13**, 765 (2017).
[44]D. F. James and D. R. Mclaren, "The laminar flow of dilute polymer solutions through porous media," J. Fluid Mech. **70**, 733 (2006).